PCCP

Cite this: *Phys. Chem. Chem. Phys.*, 2011, **13**, 2706–2713

www.rsc.org/pccp

PAPER

Molecular organization of hydrophobic molecules and co-adsorbed water in SBA-15 ordered mesoporous silica material†

Randy Mellaerts,[a] Maarten B. J. Roeffaers,[b] Kristof Houthoofd,[a] Michiel Van Speybroeck,[c] Gert De Cremer,[a] Jasper A. G. Jammaer,[a] Guy Van den Mooter,[c] Patrick Augustijns,[c] Johan Hofkens[b] and Johan A. Martens*[a]

Received 30th August 2010, Accepted 10th November 2010
DOI: 10.1039/c0cp01640c

The purpose of this study was to improve our understanding of the molecular organization of hydrophobic guest molecules in the presence of co-adsorbed water inside SBA-15 ordered mesoporous silica material. Understanding this adsorption competition is essential in the development of applications of controlled adsorption and desorption. The poorly water soluble drug compound itraconazole and the fluorescent probe Nile red were selected for the study. The interaction between itraconazole and SBA-15 was investigated using FT-IR, ^{1}H MAS NMR and ^{29}Si MAS NMR spectroscopy, by determination of adsorption isotherms and release kinetics in simulated gastric fluid. The distribution and migration of the hydrophobic fluorescent probe Nile red was visualized *in situ* using confocal fluorescence microscopy. For both molecules, there was a pronounced influence of the co-adsorbed water on adsorption, hydrophobic aggregation and migration in SBA-15 pores. These insights contribute to the development of practical methods for loading ordered mesoporous silica materials with hydrophobic molecules.

1. Introduction

Understanding adsorption and diffusion of organic guest molecules in nanosized pores of silica materials is relevant to many applications and research fields such as heterogeneous catalysis, molecular separation, bioimmobilization, fixing of organic fluorescent markers and controlled release.[1] One of the intriguing applications of ordered mesoporous silica material (OMS) is the formulation of drugs with low aqueous solubility to enhance bioavailability.[2] The pore size of OMS materials such as SBA-15 with hexagonal arrangement of cylindrical pores can be fine-tuned in the range 2 to 15 nm.[3] These pores create large surface areas suited for the adsorption of organic molecules and their delivery.[4] The use of OMS for tapping fluorescent molecules is another active research area.[5]

The majority of new chemical compounds that have been generated by drug discovery programs display poor water solubility.[6] An insufficient dissolution of these hydrophobic drugs in the gastrointestinal fluids strongly limits the oral bioavailability.[7] Ordered mesoporous silica materials such as SBA-15,[8] TUD-1[9] and FSM-16[10] have been shown to be excellent carriers for the oral delivery of hydrophobic drugs by boosting the *in vitro* dissolution and the *in vivo* uptake into the systemic circulation.[11] Since these drug delivery processes take place in aqueous environment, knowledge about the co-adsorption of water molecules is essential.

The adsorption of water molecules into the mesopores of SBA-15 ordered mesoporous silica material takes place according to a radial filling mechanism.[12] This implies that a gradual increase in the thickness of the adsorbed water layer prevails until capillary condensation takes place above a critical thickness of water film. SBA-15 material presents some inherent surface inhomogeneity that cause stronger binding of water molecules at specific sites. The interaction between various drug molecules and ordered mesoporous silica materials in the absence of water has been investigated.[13] Hydrogen bonding between the silanol groups covering the surface of ordered mesoporous silica and the polar moieties of

[a] *Centre for Surface Chemistry and Catalysis, Katholieke Universiteit Leuven, Kasteelpark Arenberg 23, BE-3001 Heverlee, Belgium. E-mail: johan.martens@biw.kuleuven.be; Fax: +32 16 321998; Tel: +32 16 321637*
[b] *Laboratory of Photochemistry and Spectroscopy, Katholieke Universiteit Leuven, Celestijnenlaan 200F, BE-3001 Heverlee, Belgium*
[c] *Laboratory for Pharmacotechnology and Biopharmacy, Katholieke Universiteit Leuven, O&N2, Herestraat 49-box 921, BE-3000 Leuven, Belgium*

† Electronic supplementary information (ESI) available: (i) Adsorption isotherms of itraconazole into SBA-15 from dichloromethane, (ii) confocal fluorescence and transmission images of SBA-15 spheres loaded with Nile red and containing a pre-adsorbed water content of 1.4 wt% after 4 h exposure to SGF, (iii) fluorescence decay measurements of Nile red adsorbed into SBA-15 spheres with a pre-adsorbed water content of 1.4 wt% and 38.5 wt% after exposure to SGF. See DOI: 10.1039/c0cp01640c

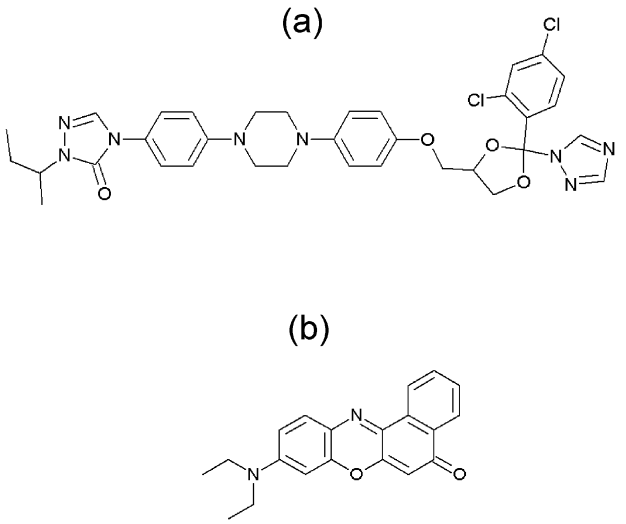

Fig. 1 Structural formula of itraconazole (a) and Nile red (b).

the adsorbed molecules play a crucial role.[14] Ibuprofen has been suggested to interact with surface silanol groups through hydrogen bonding with its carboxylic acid groups.[15] However, another study using NMR revealed ibuprofen to have liquid like mobility inside MCM-41 channels because of association of the molecules and formation of mobile dimers ruling out strong interactions with the host material.[16] Rosenholm and Linden pointed out the importance of residual silanol groups after functionalization because of their ionic dissociation in aqueous media.[17] The influence of the zeta-potential of the silica carrier and the ionic strength of the release medium on the adsorption and release of molecules has been demonstrated.[18] The release kinetics were also found to be dependent of the drug loading and the molecular arrangement of adsorbed molecules inside the pores.[19] Summarizing, previous studies indicate that the interplay of surface functionality, organic functionality and hydrophobicity of adsorbed molecules and the aqueous medium is very complicated.

We selected the hydrophobic model molecules itraconazole and Nile red and SBA-15 ordered mesoporous silica material for our investigation. The structural formula of these molecules is presented in Fig. 1. Itraconazole is a poorly water soluble drug showing solubilities of 4 μg ml^{-1} at pH 1 and less than 1 ng ml^{-1} at neutral pH.[20] Nile red is a hydrophobic fluorescent dye with a similar low aqueous solubility. Both molecules contain basic amine groups. The pK_a value of itraconazole and Nile red amounts to *ca.* 4.[21]

The impact of water molecules on both the loading and the release of itraconazole was investigated. The specific hydrogen bond interaction between itraconazole, SBA-15 and water as co-adsorbent were investigated using FT-IR, ^{1}H and ^{29}Si MAS NMR spectroscopy. These insights were used to explain the influence of the hydration degree of SBA-15 on the *in vitro* release of itraconazole into simulated gastric fluid. In a second part of the study, the hydrophobic fluorescent probe molecule Nile red adsorbed into SBA-15 with different water content was visualized with confocal fluorescence microscopy. The distribution and migration of Nile red inside SBA-15 particles when exposed to aqueous environment was investigated. In this way, it was evidenced that hydrophobic aggregation plays an important role during adsorption competition between water and Nile red inside the pores of ordered mesoporous material.

2. Experimental section

2.1 SBA-15 materials

SBA-15 powder was synthesized according to a procedure described before.[11] Briefly, 6 g of triblock copolymer Pluronic P123 (BTC-Benelux) was dissolved in 180 g of 2 M HCl. This mixture was placed in an oil bath at 35 °C under magnetic stirring. An amount of 15.3 g of sodium silicate solution (>27 wt% SiO_2, Riedel-de Haën) was diluted with 45 g demineralized water. This mixture was added dropwise to the Pluronic P123 solution under vigorous stirring. Stirring was allowed to continue for another 5 min before switching to static synthesis conditions at 35 °C. After 24 h, the silica suspension was transferred into a PTFE lined autoclave (KULeuven workshop) and placed in an oven for hydrothermal treatment at a temperature of 90 °C for another 48 h. Finally, the powder was washed on a 0.45 μm filter (Whatman Schleicher and Schuell) with demineralized water, dried and calcined at 550 °C for 8 h under ambient atmosphere to remove the triblock copolymer from the pores. An adapted synthesis procedure with the addition of CTAB was applied to obtain spherical shaped SBA-15 particles with diameters of 1–5 μm for use in confocal fluorescence microscopy.[22] Characterization of the porosity of SBA-15 powder using nitrogen adsorption revealed the presence of a total pore volume of 0.73 ml g^{-1}, divided over 0.66 ml g^{-1} of mesopores and 0.07 ml g^{-1} of micropores. The specific surface area of the mesopore walls amounted to 343 m^2 g^{-1}. The mesopore size was estimated at *ca.* 8.3 nm. Spherical shaped SBA-15 particles had a total pore volume of 0.65 ml g^{-1}, divided over 0.58 ml g^{-1} of mesopores and 0.07 ml g^{-1} of micropores. The specific surface area of the mesopore walls amounted to 366 m^2 g^{-1}. The mesopore size was estimated at *ca.* 6.3 nm.

After synthesis, SBA-15 powders and spheres were kept under controlled humidity of 0%, 52% and 97% for one week. Humidity chambers of 0%, 52% and 97% were prepared using P_2O_5 and saturated salt solutions of $Mg(NO_3)_2$ and K_2SO_4, respectively. After this equilibration period, the content of physically adsorbed water was determined using automatic Karl-Fischer titration (Metrohm). The procedure is described in the European Pharmacopeia 5.0 volume 1 method 2.5.12. We used methanol as solvent and Karl-Fischer Reagent 5 (Merck) as titrant.

2.2 Determination of itraconazole adsorption isotherms

Itraconazole (Janssen Pharmaceutica) was dissolved in dichloromethane up to a concentration of 1.25 mg ml^{-1}. This stock solution was diluted (1 : 2) three times. 20 mg of SBA-15 powder was added to 5 ml of each solution using 12 ml test tubes. The test tubes were placed in a rotary mixer (Labinco) operating at 60 rpm for 24 h. After this equilibrium period, the test tubes were centrifuged at 2500 rpm for 10 min. The precipitate was allowed to dry under vacuum at 40 °C for 48 h.

The amount of itraconazole in 1.5 ml of the dichloromethane supernatant was isolated by drying and dissolving the residue in simulated gastric fluid containing 0.5 wt% sodium laurylsulfate (Certa s.a.). The itraconazole concentration was determined using HPLC-UV. The HPLC system consisted of a LaChrom L-7100 HPLC pump, an autosampler model L-7200 equipped with a 100 µl loop, a UV detector model L-7420 set at 260 nm, and an Interface D-7000 (all Merck). UV signals were monitored and peaks were integrated using the D-7000 HSM software. The separation was performed on an RP-18 150 × 4.6 mm 5 µm Hypersil silica column (Thermo Electron Corporation) at room temperature. The mobile phase consisted of acetonitrile : tetrabutyl ammonium hydrogen sulfate 0.01 N (55 : 45 v/v), and was filtered through a 0.45 µm polytetrafluoroethylene (PTFE) membrane and degassed by ultrasonication before use. The flow rate amounted to 1.5 ml min^{-1}. The amount of SBA-15 was corrected for physically adsorbed water content of the sample.

2.3 Release of itraconazole from SBA-15

In order to study the release of itraconazole from SBA-15, the loaded powders were suspended in simulated gastric fluid without pepsin (USP XXIV) using a rotary mixer (Labinco). The amount of material in the release medium was adjusted to have a fixed maximum dose of drug substance (0.4 mg per test tube of 8 ml). At specific time intervals, the concentration of the drug substance in the dissolution medium after filtering through a 0.45 µm membrane was measured using HPLC-UV as described before.

2.4 FT-IR spectroscopy

FT-IR spectra of powders, compressed to thin films of 3 mg cm^{-2}, were recorded on a Nicolet 730 FTIR spectrophotometer (Thermo Scientific) under helium flow. Spectra were taken at 130 °C after an equilibration at this temperature for 30 min.

2.5 ^{1}H and ^{29}Si MAS NMR

The ^{1}H MAS NMR measurements were performed with a Bruker AMX300 spectrometer (7.0 T). For the acquisition of the ^{1}H MAS NMR spectra, a single-pulse excitation and spin-echo method were used. For the single-pulse excitation experiment, 32 scans were accumulated with a recycle delay of 10 s. For the spin-echo experiments, a sequence of the form θ–τ –θ–τ–aq was used, and 638 scans were accumulated with a recycle delay of 10 s. The peak amplitude at time 2τ is proportional to $\exp(-2\tau/T_2)$. Consequently the signals are attenuated, by a factor that is determined by T_2. ^{29}Si MAS NMR spectra were recorded on a Bruker Avance 400 spectrometer (9.4 T). A total of 4000 scans were accumulated with a recycle delay of 60 s. The samples were packed in 4 mm Zirconia rotors; the spinning frequency of the rotor was 5000 Hz. Tetramethylsilane (Fluka) was used as chemical shift reference in both cases.

2.6 Nitrogen adsorption

Nitrogen adsorption measurements were recorded at −196 °C on a Tristar instrument (Micromeritics). The powders were outgassed for 12 h at 40 °C before measurement. The micopore volume (V_{mi}) and the specific surface area of mesopores (S_m) were assessed using the linear region of the t-plot prior to capillary condensation. The total pore volume (V_t) and the external surface area were determined using the linear region of the t-plot following capillary condensation. The mesopore size distributions were computed from the adsorption branches of the isotherms using the Barrett–Joyner–Halenda (BJH) approach.

2.7 Confocal fluorescence microscopy

SBA-15 pretreated at a relative humidity of 0% and 97% was subsequently loaded with 10 wt% Nile red (Sigma). Nile red, which is a good sensor for the local (nano)environment,[23] was selected as the hydrophobic dye because of its low aqueous solubility similar to itraconazole. Nile red can be excited at 488 nm and its fluorescence emission was observed in the range of 500–850 nm. Both formulations of SBA-15 spheres were investigated in the dried state, as well as during immersion into simulated gastric fluid. Fluorescence intensity and transmission images of the crystals were acquired with an IX70 Olympus microscope and the Fluoview FV500 operating system (Olympus). Continuous 488 nm excitation wavelength from an Ar^{+} laser (Spectra Physics) was directed on the sample through an oil-immersion objective lens (Olympus, 100×, 1.4 NA), fluorescence being separated through a 488/543 nm dichroic mirror and a long pass filter of 505 nm (Chroma Technology). Primary analysis of the recorded images was carried out with the microscope's operating system, and a more specialized software was used for further analysis. The space-resolved emission spectra of selected parts within the individual dye-loaded silica particles were recorded using an Olympus IX70 inverted microscope. The picosecond pulsed laser light (488 nm) was directed on the back aperture and focussed through an oil-immersion lens (Olympus 100×; 1.4 NA) on the sample. These samples were mounted on a scanning stage (Physics Instruments). The fluorescence was collected by the same lens, passed through a dichroic mirror and a long pass filter, and finally focused through a 100 µm pinhole. Subsequently, the emission light was split with a non-polarizing beam splitter (50 : 50) and focused for one path into a polychromator (Spectra Pro150 Acton Research Corporation) coupled to a back illuminated liquid nitrogen cooled CCD camera (LN/CCD1340 × 400, Princeton Instruments) in order to record fluorescence spectra with a resolution down to 1 nm. The other path was focused onto an avalanche photodiode (SPCMAQ15, EG & G Electro Optics) and used to get scanning images and fluorescence decay curves (*cf.* ESI†). More details on the setup can be found elsewhere.[24]

2.8 UV absorption of powder samples

Bulk absorption spectra are recorded using a Perkin Elmer λ40 spectrophotometer equipped with a LabSphere integrating sphere. The powder sample was sandwiched between two glass plates and mounted at the back entrance of the labsphere, in order to measure the absorbance in reflectance mode.

3. Results and discussion

3.1 Itraconazole

SBA-15 powders were kept under controlled humidity for one week and the water content determined using Karl-Fischer titration. Storage at a relative humidity of 0%, 52% and 97% resulted in a SBA-15 water content of 1.4 wt%, 4.3 wt% and 38.5 wt%, respectively. The silicate connectivity of these hydrated SBA-15 powders was determined using ^{29}Si MAS NMR. The Q^n notation is convenient for indicating the number n of –OSi linkages of an Si atom. The silicate connectivity did not change with the hydration level. The Q^n distribution was *ca.* 80% Q^4, *ca.* 18% Q^3 and *ca.* 2% in Q^2. This evidences that the hydration of SBA-15 does not provoke any chemisorption or chemical modification.

Dichloromethane is an appropriate organic solvent for the loading of itraconazole into SBA-15.[2] Itraconazole was adsorbed into SBA-15 having different water content using dichloromethane solvent. The itraconazole adsorption isotherms (*cf.* ESI†) corresponded to type I isotherms according to the IUPAC classification system[25] revealing strong interaction between itraconazole and SBA-15. Saturation of the SBA-15 was reached at an itraconazole loading of *ca.* 14 wt%. The surface area that can be covered with an itraconazole molecule, estimated from the projection of a molecular model, is *ca.* 2.61 nm^2.[2] For covering the mesopore surface area SBA-15 of 343 m^2 g^{-1} with an itraconazole monolayer, a theoretical loading of 13.3 wt% would be needed. This estimate corresponds well with the experimental saturation capacity of *ca.* 14 wt% derived from the adsorption isotherm.

On the SBA-15 samples with low hydration level (1.4 wt% and 4.3 wt%) and for itraconazole loading of up to *ca.* 7.5 wt%, the itraconazole uptake from solution was quantitative. On the SBA-15 adsorbent with 38.5 wt% water content, itraconazole uptake from solution was incomplete when aiming at low loading. The saturation capacity of the 38.5 wt% water containing SBA-15 material was, however, comparable with the SBA-15 having lower water content. This high uptake of itraconazole might be the result from enhanced itraconazole solubility in the mesoconfined water phase inside the SBA-15 pores. Similar observations have been made with gas oversolubility under mesoconfinement.[26] An additional adsorption experiment was performed in which the basic molecule triethylamine was added to the itraconazole solution in dichloromethane. The amount of triethylamine amounted to about 3 times the silanol content of the SBA-15 assuming the presence of 3.7 OH groups per nm^2.[27] On 1.4 wt% hydrated SBA-15 sample triethylamine competed strongly with itraconazole for the adsorption sites. The itraconazole uptake dropped from *ca.* 14 wt% in the absence of triethylamine to *ca.* 4 wt% in its presence (*cf.* ESI†). This observation suggested the involvement of hydrogen bonding between itraconazole and SBA-15.

The carbonyl and ether groups of the itraconazole molecule present electronegative oxygen centres (Fig. 1). The electron lone pairs associated with nitrogen atoms can interact through hydrogen bonding with surface silanol groups. The interaction between itraconazole and SBA-15 after adsorption from dichloromethane and subsequent drying was investigated in more detail using FT-IR spectroscopy. In the carbonyl stretching region, itraconazole showed a free carbonyl vibration around 1700 cm^{-1} (Fig. 2). This vibration is shifted to 1680 cm^{-1} upon adsorption into SBA-15 indicating the hydrogen bonding of the carbonyl oxygen atom probably with the surface hydroxyls. The hydroxyl stretching region (Fig. 3) of unloaded SBA-15 showed a signal at 3750 cm^{-1} and a broad adsorption around 3630 cm^{-1} attributed to isolated and hydrogen bonded silanol groups, respectively. Adsorption of itraconazole caused a bathochromic shift of the silanol vibrations because of hydrogen bonding with the itraconazole carbonyl-groups. The absorption at 3750 cm^{-1} is also decreased by the shielding of the itraconazole monolayer. In the CH stretching region (Fig. 4) the adsorbed itraconazole

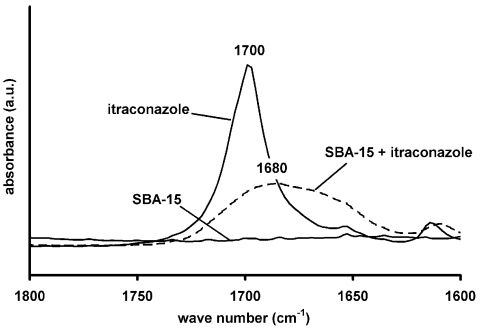

Fig. 2 FT-IR spectrum of the carbonyl stretch region (1800–1650 cm^{-1}). The carbonyl stretch of itraconazole shifts to a lower wave number when adsorbed into SBA-15 due to hydrogen bonding.

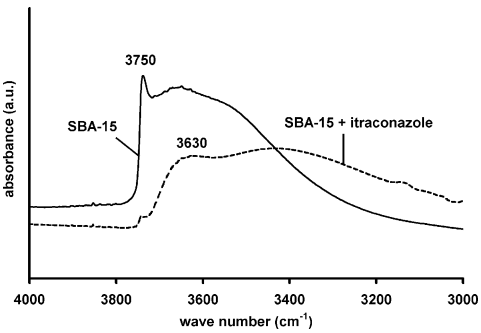

Fig. 3 FT-IR spectrum of the OH stretch region. The silanol vibrations shift to lower wave number upon adsorption of itraconazole.

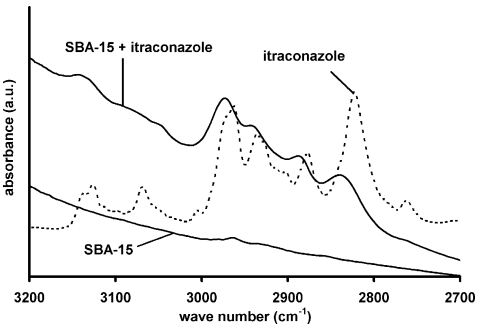

Fig. 4 FT-IR spectrum of the CH stretch region. Shifts in aliphatic vibrations are due to interaction of the neighboring O (ether) atoms and the N (piperazine) atoms with the SBA-15 surface.

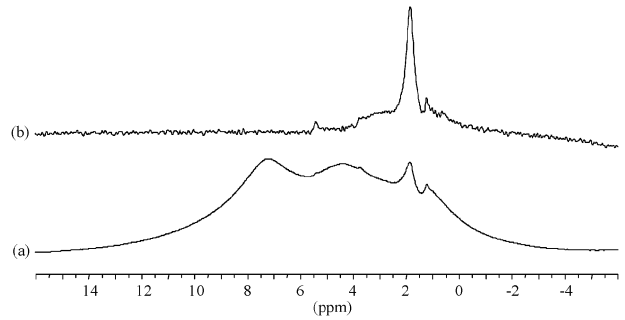

Fig. 5 ^{1}H MAS NMR spectra of SBA-15 loaded with itraconazole. The SBA-15 material was determined to have a water content of 1.4 wt% before loading. Single pulse excitation (a) and spin-echo spectrum with echo delay time of 4 ms (b).

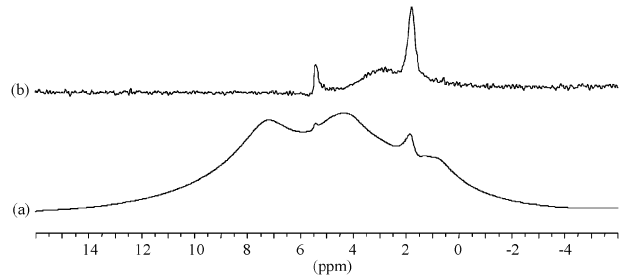

Fig. 6 ^{1}H MAS NMR spectra of SBA-15 loaded with itraconazole. The SBA-15 material was determined to have a water content of 4.3 wt% before loading. Single pulse excitation (a) and spin-echo spectrum with echo delay time of 4 ms (b).

also showed a bathochromic shift. These spectral shifts were attributed to interaction of the neighboring ether and piperazine groups with silanols. At low hydration level (1.4 wt%), itraconazole is involved in multiple hydrogen bonds with the pore walls of SBA-15.

^{1}H MAS NMR was used to gain further insight on the influence of co-adsorbed water molecules on the adsorption interaction and molecular position of itraconazole inside SBA-15. Spectra of SBA-15 loaded with itraconazole with a water content of 1.4 wt% and 4.3 wt% are presented in Fig. 5 and 6, respectively. The broad signals at 4.5 ppm and 7.2 ppm were assigned to the hydrogen atoms of the aliphatic and aromatic moieties of itraconazole, respectively. The sharp signal at 1.75 ppm was attributed to isolated surface silanols. The signal around 1 ppm corresponds to silanolic hydroxyl protons in a slightly different chemical environment, *i.e.* a different acid strength and/or location. The assignment of the signal around 5.5 ppm was more difficult. One possible explanation was the presence of water clusters; however, at a low water content of 1.4 wt%, the presence of water clusters is unlikely.[12] Another possibility was the presence of hydrogen bonded silanols which are not bonded to water molecules, as the bonding of silanols with water molecules would give rise to signals at 2.8–2.9 ppm due to chemical exchange processes between the chemically equivalent protons.[12] A more likely explanation is that part of the surface silanol protons are bound to the adsorbed itraconazole giving rise to a signal at 5.5 ppm. Grünberg *et al.* investigated hydrogen bonding of water in SBA-15 with ^{1}H MAS NMR. Based on that study, it can be assumed that the surface of SBA-15 was only partially covered with water molecules at water contents of 1.4 wt% and 4.3 wt%, while a complete coverage with multilayer build-up of water was encountered inside the pore space when the water content was increased such as in the sample with 38.5 wt% water in the present work. Remarkable is that the signal at 1.75 ppm, representing the free surface silanol groups, was very intense notwithstanding the high itraconazole loading. Itraconazole was adsorbed as a monolayer. Apparently a large part of the silanols did not find a binding partner in the monolayer. Itraconazole has a large number of possible interaction sites (Fig. 1). The electronegative oxygen atoms of the carbonyl and ether moiety were involved in the formation of hydrogen bonds with the SBA-15 surface silanol groups as evidenced with FT-IR (Fig. 4). However, a large part of the silanol groups was inaccessible for bulky adsorbed molecules presumably because of the roughness of the SBA-15 surface.[27] The ^{1}H MAS NMR spectrum of SBA-15 with a water content of 4.3 wt% loaded with itraconazole is depicted in Fig. 6. Compared with the spectrum at lower hydration level (Fig. 5) the signal at 5.5 ppm was increased, while the signal at 1.75 ppm was decreased. This can be attributed to the formation of water clusters on silanol groups. Water clusters are proposed to be positioned between the itraconazole molecules and the SBA-15 surface. The transverse relaxation time (T2) of the signal at 7.2 ppm was used to estimate the mobility of itraconazole molecules. T2 amounted to 0.285 ms and 0.308 ms for the itraconazole loaded SBA-15 samples with a water content of 1.4 wt% and 4.3 wt%, respectively. Thus the mobility of itraconazole was slightly increased at higher water content. When compared to previous work dealing with ibuprofen adsorbed into MCM-41 presenting T2 values between 2.4 and 16.6 ms,[28] the mobility of itraconazole in SBA-15 remains rather limited. When the water content was further increased to 38.5 wt%, the ^{1}H MAS NMR spectrum consisted of overlapped broad peaks and could not be interpreted.

Itraconazole release from SBA-15 containing co-adsorbed water was evaluated *in vitro* using simulated gastric fluid (Fig. 7). Significant differences were observed depending on the water content of the itraconazole–SBA-15 formulation. The released itraconazole fraction amounted to 3%, 15% and 70% for the SBA-15 materials having a water content of 1.4 wt%, 4.3 wt% and 38.5 wt%, respectively. This experiment

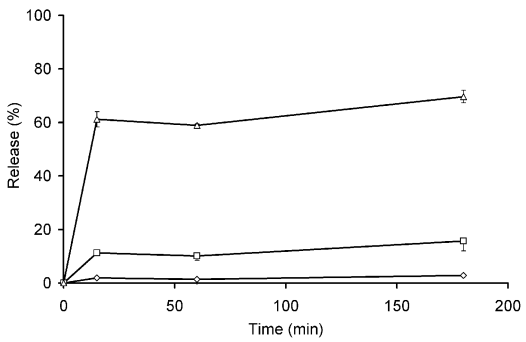

Fig. 7 Release of itraconazole from SBA-15 having different pre-adsorbed water content: 38.5 wt% (△), 4.3 wt% (□), 1.4 wt% (◇). Symbols indicate avs ± sd (n = 3).

revealed that co-adsorbed water assists the release of itraconazole in simulated gastric fluid. This observation might look surprising at first sight as it might be expected that water molecules from simulated gastric fluid rule out the influence of the co-adsorbed water molecules already present before immersion. However, a very plausible explanation for this behavior is the positioning of water molecules between itraconazole and the SBA-15 surface as derived from ^{1}H MAS NMR. The water molecules lift the itraconazole molecules from the surface facilitating desorption upon exposure to aqueous environment. These observations clearly support the idea that the release of hydrophobic itraconazole drug from SBA-15 highly depends on the initial adsorbed state of itraconazole in the SBA-15 pores. And that co-adsorbed water molecules impact this adsorbed state and consequently the release or pharmaceutical performance.

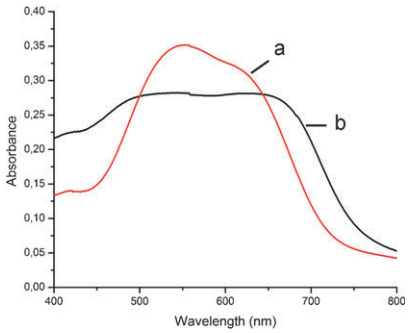

Fig. 8 Bulk absorption spectra of SBA-15 spheres loaded with 10 wt% NR and pre-adsorbed water content of 38.5 wt% (a) and 1.4 wt% (b).

3.2 Nile red

The solvatochromic dye Nile was selected as second hydrophobic model molecule in this study and loaded into SBA-15 ordered mesoporous silica material. This fluorescent probe enables us to visualize the distribution and migration inside the SBA-15 pores at the micro-scale using confocal fluorescence microscopy.[29] Nile red has a limited aqueous solubility similar to itraconazole and its strong spectral response to changes in the (nano)environment makes it an ideal probe for visualization of dynamic processes.[30] Recently, the diffusion of the anticancer drug doxorubicin was investigated in thin mesoporous silica films.[31]

SBA-15 with a water content of 1.4 wt% and 38.5 wt% were loaded with 10 wt% Nile red. Since it is known that both absorption and emission bands of Nile red show strong polarity dependence, bulk absorption spectra were recorded first (Fig. 8). The pronounced influence of the co-adsorbed water content is clearly visible in these spectra. The presence of large amounts of water results in a strong blue shift; this shift can be explained as water molecules in close interaction with Nile red dye molecules shield the effect of the SBA-15 host. Similar spectral behavior has been observed before with Nile red in siliceous zeolites. The exposure of these samples to polar vapors, such as ethanol and acetone, caused similar blue-shifts.[32] Confocal fluorescence microscopy images of SBA-15 spheres loaded with 10 wt% Nile red having pre-adsorbed water content of 38.5 wt% and 1.4 wt% are shown in Fig. 9a and 10a, respectively. The loading with Nile red yielded in both cases homogeneous fluorescence emission intensity over the SBA-15 particles. Since both absorbance and emission are strongly susceptible to changes in the local

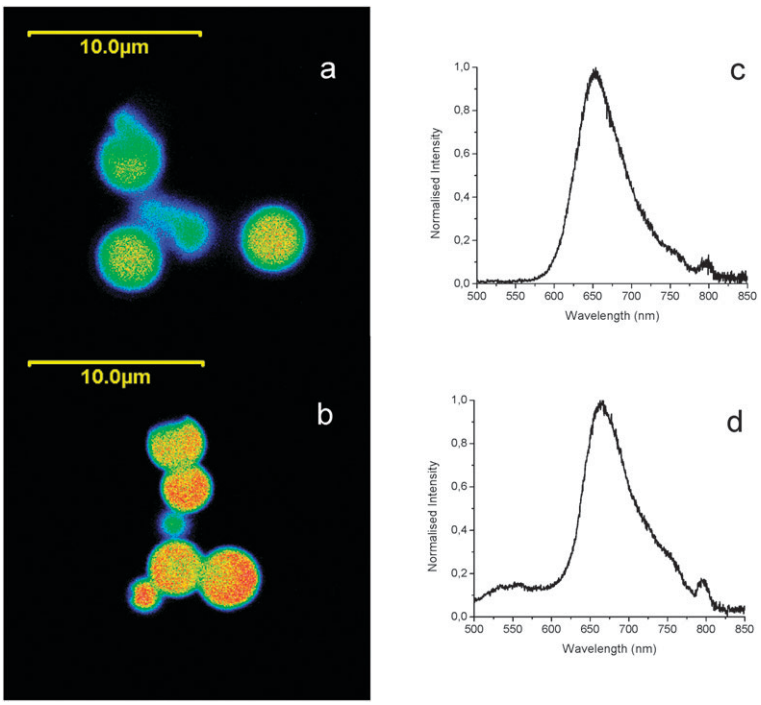

Fig. 9 Confocal fluorescence microscopy imaging (left) and corresponding emission spectra (right) of Nile red loaded into SBA-15 spheres with pre-adsorbed water content of 38.5 wt%. Dried state (a and c) and after exposure to simulated gastric fluid for 10 min (b and d).

environment, fluorescence spectra were recorded at the particle's edge and centre. The microscope's spatial resolution of *ca*. 300 nm enabled us to distinguish between both regions of the μm sized SBA-15 particles. Within one type of sample, no dramatic differences were observed. The emission of the SBA-15 particles with low water content peaks around 660–680 nm and the samples with large amounts of co-adsorbed water have a slightly blue-shifted emission maximum around 655 nm. These observations support a homogeneous dye distribution throughout the SBA-15 particle.

The fluorescent emission was subsequently monitored upon contact of the Nile red loaded SBA-15 samples with simulated gastric fluid (SGF, pH 1.2). Fig. 9b presents the temporal changes in the fluorescence intensity of the Nile red loaded SBA-15 spheres with co-adsorbed water content of 38.5 wt%. Upon suspension into simulated gastric fluid, the fluorescence intensity increased rapidly and progressed within 10 minutes from the rim toward the core of the SBA-15 particles. This increase of fluorescence emission is accompanied with a 10 nm red-shift (Fig. 9c and d). On first sight this increase in fluorescence over the whole SBA-15 particle seems to be contradictory with the expected release of Nile red molecules from the SBA-15 host. However, as shown before, the presence of water molecules induces a blue shift in the light absorption which results in a more efficient excitation at 488 nm.

When these experiments are repeated with SBA-15 with only 1.4 wt% water co-adsorbed with Nile red (Fig. 10b), the fluorescence pattern did not change very rapidly. Only after long exposure (1 h) to SGF, the fluorescence intensity increased strongly (much stronger than in the previous sample) near the outer surface of the SBA-15 particles. This increased emission intensity is accompanied with a 10 nm red-shift (Fig. 10c and d). The increased fluorescent emission was interpreted as being caused by hydrophobic aggregation of Nile red molecules forced by the influx of water. The ultrafast fluorescence decay measured in this sample seems to support this idea. Whereas Nile red in the SBA-15 with 38.5 wt% pre-adsorbed water has a decay of 0.6 ns before and 0.6–1 ns after exposure to SGF, in this sample the fluorescence decay after contact with SGF is very fast, not resolvable from the instrument response function (decay faster than ±500 ps).

It can be assumed that hydrophobic aggregation visualized with Nile red also occurs in the case of itraconazole and contributes to the decreased release of itraconazole from SBA-15 with low co-adsorbed water content. Only after very long exposure times to SGF of 4 h and more, Nile red molecules released into the SGF tended to crystallize into needles at the outer surface due to the limited solubility (*cf*. ESI†).

The observations with Nile red confirm the importance of co-adsorbed water that acts as a sort of lubricating agent by avoiding strong hydrophobic interactions between NR molecules and helping hydrophobic molecules to exit rapidly from the SBA-15 host upon contact with SGF.

4. Conclusions

In this study, we revealed the organization of hydrophobic guest molecules itraconazole and Nile red with SBA-15 ordered mesoporous silica material in the presence of co-adsorbed water molecules. At low SBA-15 hydration level, itraconazole is involved in multiple hydrogen bonding with the pore walls of SBA-15. With increasing co-adsorbed water

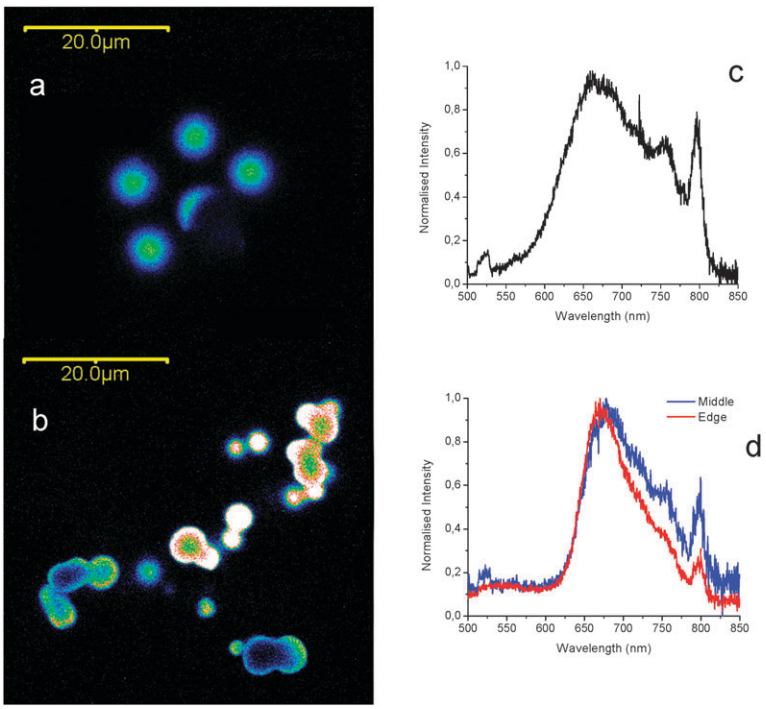

Fig. 10 Confocal fluorescence microscopy imaging (left) and corresponding emission spectra (right) of Nile red loaded into SBA-15 spheres with pre-adsorbed water content of 1.4 wt%. Dried state (a and c) and after exposure to simulated gastric fluid for 1 h (b and d).

content, water clusters positioned between itraconazole and the SBA-15 surface decrease the host–guest interaction. The amount of itraconazole rapidly released from SBA-15 when exposed to simulated gastric fluid increases drastically with increasing co-adsorbed water content. Using confocal fluorescence microscopy, the distribution and migration of the hydrophobic molecule Nile red was visualized inside the SBA-15 pores. The co-adsorbed water content has a pronounced influence on the migration pattern of Nile red inside the pore space when exposed to simulated gastric fluid. Hydrophobic aggregation of Nile red near the outer surface of SBA-15 acts as a barrier for the incoming water molecules when the initial co-adsorbed water content is low. When SBA-15 contained higher amounts of co-adsorbed water, the influx of water progresses rapidly to the centre of SBA-15 particles, causing a more complete release of guest molecules. To conclude, we revealed that the adsorbed state of itraconazole and the hydrophobic aggregation behaviour of Nile red inside the SBA-15 pore space highly depends on co-adsorbed water. These effects should be kept in mind in applications of ordered mesoporous silica materials as carriers for poorly water soluble molecules.

Acknowledgements

R. Mellaerts and M. B. J. Roeffaers acknowledge the Flemish FWO for a post-doctoral fellowship. M. Van Speybroeck acknowledges the Flemish IWT for a PhD grant. G. De Cremer acknowledges the FWO for a PhD grant. We thank Stephanie Vandenwaeyenberg for assistance during Karl-Fischer titration. The work was carried out in a KU Leuven interdisciplinary research project (IDO) and was supported by an industrial research fund (IOF). J. Martens acknowledges the Flemish government for long term structural funding (Methusalem). The topic of controlled release is investigated in Interuniversity Attraction Poles (IAP-PAI).

Notes and references

1 D. Bruehwiler, G. Calzaferri, T. Torres, J. H. Ramm, N. Gartmann, L.-Q. Dieu, I. Lopez-Duarte and M. Victoria Martinez-Diaz, *J. Mater. Chem.*, 2009, **19**, 8040; M. Vallet-Regi, A. Ramila, R. P. del Real and J. Perez-Pariente, *Chem. Mater.*, 2001, **13**, 308.
2 R. Mellaerts, C. A. Aerts, J. Van Humbeeck, P. Augustijns, G. Van den Mooter and J. A. Martens, *Chem. Commun.*, 2007, 1375; I. Izquierdo-Barba, E. Sousa, J. C. Doadrio, A. L. Doadrio, J. P. Pariente, A. Martinez, F. Babonneau and M. Vallet-Regi, *J. Sol–Gel Sci. Technol.*, 2009, **50**, 421.
3 J. S. Beck, J. C. Vartulli, W. J. Roth, M. E. Leonowicz, C. T. Kresge, K. D. Schmitt, C. T. W. Chu, D. H. Olson, E. W. Sheppard, S. B. McCullen, J. B. Higgins and J. L. Schlenker, *J. Am. Chem. Soc.*, 1992, **114**, 10834; D. Y. Zhao, J. L. Feng, Q. S. Huo, N. Melosh, G. H. Fredrickson, B. F. Chmelka and G. D. Stucky, *Science*, 1998, **279**, 548.
4 S. B. Wang, *Microporous Mesoporous Mater.*, 2009, **117**, 1; S. P. Rigby, M. Fairhead and C. F. van der Walle, *Curr. Pharm. Des.*, 2008, **14**, 1821; M. Vallet-Regi, F. Balas and D. Arcos, *Angew. Chem., Int. Ed.*, 2007, **46**, 7548; M. Danilczuk, K. Dlugopolska, T. Ruman and D. Pogocki, *Mini-Rev. Med. Chem.*, 2008, **8**, 1407; S. P. Hudson, R. F. Padera, R. Langer and D. S. Kohane, *Biomaterials*, 2008, **29**, 4045.
5 H. Maas, A. Currao and G. Calzaferri, *Angew. Chem., Int. Ed.*, 2002, **41**, 2495.
6 Report by Technology Catalysts International Corporation, Delivery of Poorly Soluble drugs, Falls Church, VA, 3rd edn, 2002.
7 C. A. Lipinski, F. Lombardo, B. W. Dominy and P. J. Feeney, *Adv. Drug Delivery Rev.*, 1997, **23**, 3.
8 M. Van Speybroeck, V. Barillaro, T. Do Thi, R. Mellaerts, J. Martens, J. Van Humbeeck, J. Vermant, P. Annaert, G. Van den Mooter and P. Augustijns, *J. Pharm. Sci.*, 2008, **98**, 2648.
9 T. Heikkila, J. Salonen, J. Tuura, M. S. Hamdy, G. Mul, N. Kumar, T. Salmi, D. Y. Murzin, L. Laitinen, A. M. Kaukonen, J. Hirvonen and V. P. Lehto, *Int. J. Pharm.*, 2007, **331**, 133.
10 Y. Tozuka, A. Wongmekiat, K. Kimura, K. Moribe, S. Yamamura and K. Yamamoto, *Chem. Pharm. Bull.*, 2005, **53**, 974.
11 R. Mellaerts, R. Mols, P. Kayaert, P. Annaert, J. Van Humbeeck, G. Van den Mooter, J. A. Martens and P. Augustijns, *Int. J. Pharm.*, 2008, **357**, 169; R. Mellaerts, R. Mols, J. A. G. Jammaer, C. A. Aerts, P. Annaert, J. Van Humbeeck, G. Van den Mooter, P. Augustijns and J. A. Martens, *Eur. J. Pharm. Biopharm.*, 2008, **69**, 223.
12 B. Grünberg, T. Emmler, E. Gedat, I. Shenderovich, G. H. Findenegg, H. H. Limbach and G. Buntkowsky, *Chem.–Eur. J.*, 2004, **10**, 5689.
13 W. Xia and J. Chang, *J. Controlled Release*, 2006, **110**, 522; Z. Wu, Y. Jiang, T. Kim and K. Lee, *J. Controlled Release*, 2007, **119**, 251; C. Charnay, S. Bégu, C. Tourné-Peteilh, L. Nicole, D. A. Lerner and J. M. Devoiselle, *Eur. J. Pharm. Biopharm.*, 2004, **57**, 533; A. Vinu, M. Miyahara and K. Ariga, *J. Nanosci. Nanotechnol.*, 2006, **6**, 1510.
14 E. Papirer, *Adsorption on Silica Surfaces*, 2000, p. 63.
15 S. W. Song, K. Hidajat and S. Kawi, *Langmuir*, 2005, **21**, 9568.
16 F. Babonneau, L. Yeung, N. Steunou, C. Gervais, A. Ramila and M. Vallet-Regi, *J. Sol–Gel Sci. Technol.*, 2004, **31**, 219.
17 J. M. Rosenholm and M. Linden, *J. Controlled Release*, 2008, **128**, 157.
18 Z. J. Wu, H. Xiang, T. Kim, M. S. Chun and K. Lee, *J. Colloid Interface Sci.*, 2006, **304**, 119.
19 R. Mellaerts, J. A. G. Jammaer, M. Van Speybroeck, H. Chen, J. Van Humbeeck, P. Augustijns, G. Van den Mooter and J. A. Martens, *Langmuir*, 2008, **24**, 8651.
20 K. Six, T. Daems, J. de Hoon, A. Van Hecken, M. Depre, M. P. Bouche, P. Prinsen, G. Verreck, J. Peeters, M. E. Brewster and G. Van den Mooter, *Eur. J. Pharm. Sci.*, 2005, **24**, 179.
21 D. L. Sacket and J. Wolff, *Anal. Biochem.*, 1987, **167**, 228.
22 A. Katiyar, S. Yadav, P. G. Smirniotis and N. G. Pinto, *J. Chromatogr., A*, 2006, **1122**, 13.
23 A. K. Dutta, K. Kamada and K. Ohta, *J. Photochem. Photobiol., A*, 1996, **93**, 57.
24 M. Cotlet, J. Hofkens, S. Habushi, G. Dirix, M. Van Guyse, J. Michiels, J. Vanderleyden and F. C. De Schryver, *Proc. Natl. Acad. Sci. U. S. A.*, 2001, **98**, 14398; M. Maus, E. Rousseau, M. Cotlet, G. Schweizer, J. Hofkens, M. Van der Auweraer, F. C. De Schryver and A. Krueger, *Rev. Sci. Instrum.*, 2001, **72**, 36.
25 IUPAC Recommendations, *Pure Appl. Chem.*, 1994, **66**, 1739.
26 S. Miachon, V. V. Syakaev, A. Rakhmatullin, M. Pera-Titus, S. Caldarelli, Stefano and J.-A. Dalmon, *ChemPhysChem*, 2008, **9**, 78.
27 I. G. Shenderovich, G. Buntkowsky, A. Schreiber, E. Gedat, S. Sharif, J. Albrecht, N. S. Golubev, G. H. Findenegg and H. H. Limbach, *J. Phys. Chem. B*, 2003, **107**, 11924.
28 T. Azais, C. Tourne-Peteilh, F. Aussenac, N. Baccile, C. Coelho, J. M. Devoisselle and F. Babonneau, *Chem. Mater.*, 2006, **18**, 6382.
29 M. B. J. Roeffaers, G. De Cremer, H. Uji-i, B. Muls, B. F. Sels, P. A. Jacobs, F. C. De Schryver, D. E. De Vos and J. Hofkens, *Proc. Natl. Acad. Sci. U. S. A.*, 2007, **104**, 12603.
30 G. Hungerford and J. A. Ferreira, *J. Lumin.*, 2001, **93**, 155.
31 T. Lebold, C. Jung, J. Michaelis and C. Braeuchle, *Nano Lett.*, 2009, **9**, 2877.
32 J. L. Meinershagen and T. Bein, *J. Am. Chem. Soc.*, 1999, **121**, 448.